Chemistry of Metals and Alloys

Chem. Met. Alloys 2 (2009) 59-67
Ivan Franko National University of Lviv
www.chemetal-journal.org

Hydrogenation of $Ti_{4-x}Zr_xFe_2O_y$ alloys and crystal structure analysis of their deuterides

I.Yu. ZAVALIY[1]*, R.V. DENYS[1], I.V. KOVAL'CHUCK[1], A.B. RIABOV[1], R.G. DELAPLANE[2]

[1] *Physico-Mechanical Institute of National Academy of Sciences of Ukraine, 5, Naukova St., 79601 Lviv, Ukraine*
[2] *Studsvik Neutron Research Laboratory, Uppsala University, SE-611 82 Nyköping, Sweden*
** Corresponding author. Tel.: +380-322-654833; fax +380-322-649427; e-mail: zavaliy@ipm.lviv.ua*

Received May 15, 2009; accepted June 30, 2009; available on-line November 16, 2009

The crystal structure of four saturated deuterides of oxygen-modified intermetallic compounds $Ti_{4-x}Zr_xFe_2O_y$ (x = 1, 2, 3; y = 0.25, 0.5) has been investigated by both X-ray and neutron powder diffraction. The distribution of D-atoms in the metal matrix has been determined and analysed as function of the Ti/Zr and oxygen content. The obtained crystallographic data were compared with structural results for other oxygen-stabilised Ti/Zr-based η-phases.

Titanium and zirconium alloys / Metal hydrides / Crystal structure / X-ray diffraction / Powder neutron diffraction

1. Introduction

Ti–Fe-based alloys are among the easiest available and most inexpensive hydrogen storage materials. In the Ti–Fe system there is only one hydrogen absorbing intermetallic compound, TiFe, with the CsCl type of structure [1]. Hydrogenation of this compound leads to the formation of the $TiFeH_{\sim1}$ hydride under ambient and the $TiFeH_{\sim1.9}$ hydride under elevated hydrogen pressures [2,3]. The hydrogen absorption properties of TiFe-based materials have been the focus of many investigations. Some of them observed substantial improvement of hydrogenation activation parameters (as compared with oxygen-less alloys) by the presence of the oxygen-stabilized η-$Ti_{4-x}Fe_xO_y$ phase [4,5]. This phase is characterized by the η-Fe_3W_3C type of structure (insertion derivative of the Ti_2Ni type), variable oxygen concentration and Ti/Fe solid solution between A_2B and equiatomic compositions [5]. In its turn, the hydrogenation capacity of the η-$Ti_{4-x}Fe_{2+x}O_y$ phase, which is able to absorb hydrogen at room temperature, substantially depends on both the oxygen content and the Ti/Fe ratio. It has been shown [5] that an increase of the oxygen content from 7 to 14 at.% in the $Ti_4Fe_2O_x$ compound is accompanied by a decrease of the hydrogenation capacity from 5.75 to 1.56 H/f.u. The structures of the $Ti_4Fe_2O_{0.4}$ compound and the $Ti_4Fe_2OD_{2.25}$ deuteride have been studied in details [6,7].

The Zr_2Fe compound, crystallizing in the $CuAl_2$ structure type, exists in the 1050-1250 K temperature range [8]. The oxygen-stabilized η-phase $Zr_4Fe_2O_x$ (x = 0.25-0.6), crystallizing in the η-Fe_3W_3C structure type, forms at temperatures above 1270 K [9]. Both these materials are efficient hydrogen absorbers, however, the oxygen-stabilized η-phase reveals interesting peculiarities during hydrogenation: it is more stable against disproportionation in hydrogen than the Zr_2Fe compound [10-12]. As for the $Ti_4Fe_2O_x$ compound, the hydrogenation capacity of $Zr_4Fe_2O_x$ strongly depends on the oxygen content and increases from ~7.7 H/$Zr_4Fe_2O_{0.6}$ to 9.4 H/$Zr_4Fe_2O_{0.3}$ [13,14]. Because of the low pressure of the hydrogen absorption-desorption plateau, the Zr_2Fe alloy is used only as a getter.

Since isostructural O-stabilized η-phases exist in both the Ti–Fe–O and Zr–Fe–O system, and by analogy with the Ti–Zr–Ni–O alloys [15], we have predicted the existence of a continuous solid solution between these phases in the Ti–Zr–Fe–O system. The aim of this work was the experimental observation of the continuous solid solution and the influence of oxygen on the hydrogenation properties of the alloys. A study of deuterated η-$Ti_{4-x}Zr_xFe_2O_{0.25-0.5}$ phases by XRD and PND allowed us to determine the distribution of the D atoms as function of the Ti/Zr ratio and oxygen content.

2. Experimental

$Ti_4Fe_2O_x$, $Ti_3ZrFe_2O_x$, $Ti_2Zr_2Fe_2O_x$ and $TiZr_3Fe_2O_x$ (x = 0.25-0.5) alloys were prepared from high-purity compact metals (≥99.9%) and compacted powders of TiO_2 or ZrO_2 oxide by arc melting in purified argon.

Table 1 Crystallographic parameters of $Ti_{4-x}Zr_xFe_2O_y$ compounds and the corresponding hydrides (deuterides).

Compound	*a*, Å	*V*, Å^3	Hydride	*a*, Å	*V*, Å^3	Δ*V*/*V*, %	Δ*V*/at.H, Å^3
$Ti_4Fe_2O_{0.25}$	11.3355(2)	1456.54(9)	$Ti_4Fe_2O_{0.25}D_{4.9}$	11.6838(1)	1594.96(3)	9.50	1.77
$Ti_4Fe_2O_{0.5}$	11.3306(8)	1454.7(3)	$Ti_4Fe_2O_{0.5}D_{3.5}$	11.6843(1)	1595.19(3)	9.66	2.51
$Ti_3ZrFe_2O_{0.5}$	11.5771(7)	1551.7(3)	$Ti_3ZrFe_2O_{0.5}H_5$	12.0413(4)	1745.9(2)	12.52	2.43
$Ti_2Zr_2Fe_2O_{0.25}$	11.836(1)	1658.1(6)	$Ti_2Zr_2Fe_2O_{0.25}D_{7.2}$	12.4090(5)	1910.8(1)	15.24	2.19
$Ti_2Zr_2Fe_2O_{0.5}$	11.805(2)	1645.3(9)	$Ti_2Zr_2Fe_2O_{0.5}D_{5.8}$	12.2982(3)	1860.0(6)	13.05	2.31
$TiZr_3Fe_2O_{0.5}$	12.015(1)	1734.4(4)	$TiZr_3Fe_2O_{0.5}H_{6.8}$	12.5881(7)	1994.7(3)	15.01	2.39
$Zr_4Fe_2O_{0.25}$ *	12.2183(7)	1824.1(3)	$Zr_4Fe_2O_{0.25}D_{9.9}$	13.0714(2)	2233.40(6)	22.44	2.58
$Zr_4Fe_2O_{0.5}$ *	12.236(1)	1832.2(5)	$Zr_4Fe_2O_{0.5}D_{8.1}$	12.9864(6)	2190.1(2)	19.53	2.76

For the comparison, the table contains in addition values for parent η-$Zr_4Fe_2O_x$ compounds (marked by asterisk, x = 0.25, 0.5) and their hydrides, the structure and properties of which will be published elsewhere.

The as-cast alloys were annealed in vacuum at 980°C for 5 days. Hydrogenation was performed at room temperature in an autoclave under 0.1-0.15 MPa hydrogen pressure after preliminary activation of the samples by heating at 500°C for 15 min. The amount of absorbed hydrogen was measured volumetrically. Phase-structural analysis of the alloys and their hydrides (deuterides) was performed on XRD data collected on DRON-3.0 (Cu Kα) and Bruker D8 (Cu Kα) diffractometers. The structures of the deuterides were studied by powder neutron diffraction, on data collected at the Neutron Research Laboratory of Uppsala University (Studsvik, Sweden) with the use of NPD (λ = 1.47 Å) and R2D2 (λ = 1.55 Å) diffractometers. The structures were refined by full-profile Rietveld analysis using CSD and GSAS programs [16,17].

3. Results and discussion

The formation of single-phase alloys with $Ti_4Fe_2O_x$, $Ti_3ZrFe_2O_x$, $Ti_2Zr_2Fe_2O_x$ and $TiZr_3Fe_2O_x$ (x = 0.25-0.5) composition confirms our assumption about the existence of a continuous $Ti_4Fe_2O_x$–$Zr_4Fe_2O_x$ solid solution. The lower limit of this solid solution corresponds to x = 0.25-0.3, whereas the upper studied oxygen concentration limit was x = 0.5. The existence of substituted η-phases with higher oxygen content (0.6-1.0) can be predicted considering the maximum hydrogen contents in the $Zr_4Fe_2O_{0.6}$ and Ti_4Fe_2O suboxides. Hydrogenation of $Ti_4Fe_2O_x$, $Ti_3ZrFe_2O_x$, $Ti_2Zr_2Fe_2O_x$ and $TiZr_3Fe_2O_x$ alloys revealed that all of them absorb substantial amounts of hydrogen (from 3.5 to 7.2 H atoms per formula unit). Upon hydrogenation the metal matrix of the compounds preserves the cubic structure of the Ti_2Ni (η-Fe_3W_3C) type; the expansion of the unit cell reaches 9.5-17.3%, corresponding to 1.77-2.51 Å^3 per one absorbed D atom. The refined crystallographic parameters of the parent η-phases and their saturated hydrides (deuterides) are provided in Table 1. For comparison, the table contains in addition values for the parent η-$Zr_4Fe_2O_x$ compounds (x = 0.25, 0.5) and their hydrides, the structure and properties of which will be published elsewhere.

As expected, an increase of the oxygen content leads to a decrease of the hydrogenation capacity, whereas the same hydrogenation capacity increases with Zr→Ti substitution. The main factors influencing the structure of the hydrogen sublattice are the size of the interstices and their surrounding. Changes in the size of the interstices caused by the replacement of Ti by larger Zr atoms produce changes in the hydrogenation capacity. The increase of the overall volume of the interstices (calculated by the rigid ball model for r_{Zr} = 1.602 Å, r_{Ti} = 1.462 Å, r_{Fe} = 1.274 Å) with increasing Zr content is illustrated in Fig. 1.

The hydrogenation capacity of $Ti_{4-x}Zr_xFe_2O_{0.5}$ alloys *vs.* the Zr content is plotted in Fig. 2. The dependence of the lattice parameters on the Zr content for the initial compounds of the $Ti_{4-x}Zr_xFe_2O_{0.5}$ sequence and their hydrides is shown in Fig. 3. It is clear that the increase of the volume of the interstices caused by Ti→Zr substitution changes the equilibrium hydrogen dissociation pressure in the alloy-hydrogen system, inducing a transition of the properties from a typical hydrogen storage (Ti-based compounds) to a getter material (Zr-based compounds).

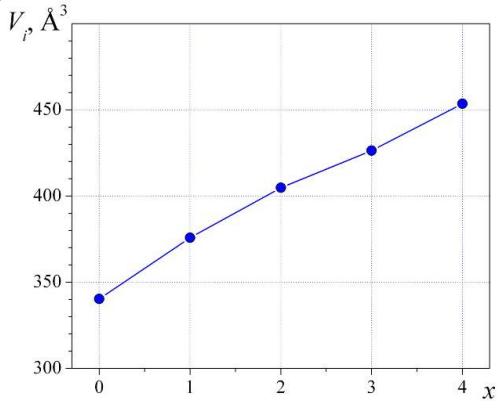

Fig. 1 Dependence of the total volume of interstices on the Zr content in $Ti_{4-x}Zr_xFe_2O_{0.5}$ alloys.

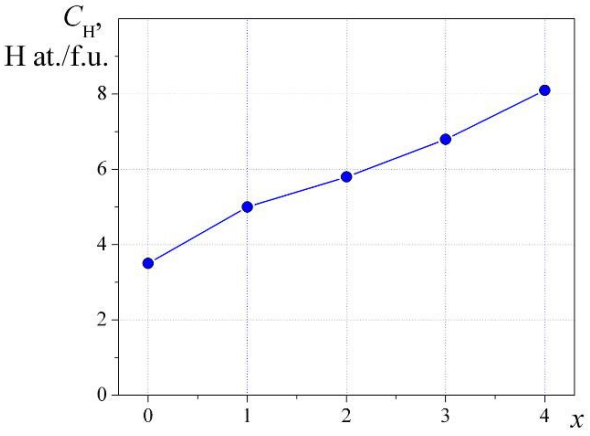

Fig. 2 Hydrogenation capacity of $Ti_{4-x}Zr_xFe_2O_{0.5}$ alloys *vs.* Zr content.

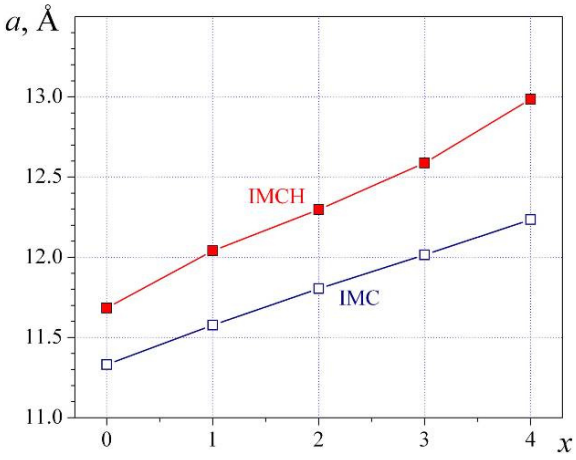

Fig. 3 Dependence of the lattice parameters of $Ti_{4-x}Zr_xFe_2O_{0.5}$ compounds (IMC) and their hydrides (IMCH) on the Zr content.

Using powder X-ray and neutron diffraction analysis we have studied the structures of deuterides of Ti-based ($Ti_4Fe_2O_x$) and partially substituted Ti-Zr-based ($Ti_2Zr_2Fe_2O_x$) η-phases with different oxygen content (x = 0.25, 0.5). X-ray and neutron diffraction patterns for some of the studied deuterides, refined by the full-profile Rietveld method, are presented in Figs. 4-6.

Fig. 7 shows 1/8 of the unit cell of the structure of the η-phase, in which all types of tetrahedral, octahedral and triangular interstices are shown. The notation for the interstices used in our work corresponds to that proposed in earlier studies of isostructural hydrides [18-21]. The triangular interstice between the D7 octahedron and D1 tetrahedron, filling of which has not been reported before, is marked as T2. The results of the structure refinement for the deuterides are given in Table 2. The number of deuterium atoms in different positions and the total number per unit cell in the studied deuterides is provided in Table 3. Relevant data for $Ti_4Fe_2OD_{2.5}$ are taken from [7].

The structure of the hydrogen sublattice in the studied oxygen-stabilized η-phases obeys the principles of the crystal chemistry of metal hydrides: a) the radii of occupied interstices exceed 0.40 Å; b) all H–H distances are at least 2.0 Å; c) interstices formed by active hydrogen-forming metals (Ti, Zr) are filled in the first turn. However, the strongest impact on the H-capacity and distribution of H atoms is provided by O-H blocking, the distance of which should be at least 2.6 Å [21].

It can be seen from the refined structural data (Tables 2,3) that hydrogen atoms fill tetrahedral [M_3Fe] – D1 (32*e*), D2 (192*i*) and D3 (96*g*) as well as octahedral interstices [M_6] – D7 (8*a*). Other types of interstice, namely tetrahedral [M_2Fe_2] – D4; [MFe_3] – D6 and [Fe4] – D5 are not favourable for the insertion of hydrogen atoms. In our work we have also observed filling of the triangular faces T1 and T2 [$M1_3$], situated between the interstices D7/D8 and D7/D1, respectively. The sizes of these interstices depend on the level of zirconium substitution for titanium, therefore we observed filling of these interstices only for $Ti_2Zr_2Fe_2O_x$ compositions (x = 0.25, 0.5). At equal content of Ti and Zr the filling of triangular faces depends on the oxygen content in the alloy, which is reflected in the hydrogenation capacity of these alloys. D2 and D3, the most occupied sites in the studied hydrides, have the radii r = 0.35 Å in the parent Ti-based alloys. In the Zr-substituted compounds r_{D2} = 0.42-0.44 Å and r_{D3} = 0.46-0.48 Å, respectively. Filling of $(Zr,Ti)_6$ octahedra by D atoms was observed in all studied compounds $Ti_4Fe_2O_x$ and $Ti_2Zr_2Fe_2O_x$ (x = 0.25, 0.5). The diagrams in Fig. 8 show the distribution of D-atoms among the different interstices.

Generalizing the results of the structural studies we should first emphasize that the hydrogen sublattice in all studied hydrides is disordered, similarly to other earlier studied hydrides of η-phases. This is caused by partial filling of oxygen positions in octahedral interstices. Because of the repulsion between hydrogen atoms (H–H blocking) and between H and O atoms (O–H blocking) the other interstices are also partly filled. The decrease of the oxygen content in the compounds and the occupancy of these octahedral interstices is accompanied by an increase of the number of interstices that can be filled by hydrogen. For example, the hydrogenation capacity of the $Ti_4Fe_2O_x$ compound, in which only two interstices (D7 and D3) are large enough to accommodate hydrogen atoms (≥0.40 Å), can be expressed by the formula: $C_H = (n_{D7}+n_{D3}\times(1-x))/16$, where C_H is the capacity per formula unit; x the oxygen content; n_i the site multiplicities (n_{D7} = 8, n_{D3} = 96). Capacity values calculated by this formula agree well with the experimental data. The decrease of the hydrogen content with increasing oxygen content can be

Table 2 Atomic parameters for saturated deuterides of $Ti_{4-x}Zr_xFe_2O_y$ alloys, space group $Fd\bar{3}m$, origin at $\bar{3}m$. The radii of filled interstices (r_i,) are calculated by the rigid ball model using atomic radii of *M*1 and *M*2, averaged taking into account the site occupation by Zr/Ti.

		$Ti_4Fe_2O_{0.25}D_{4.9}$	$Ti_4Fe_2O_{0.5}D_{3.5}$	$Ti_2Zr_2Fe_2O_{0.25}D_{7.2}$	$Ti_2Zr_2Fe_2O_{0.5}D_{5.8}$
Lattice parameter	*a*, Å	11.6838(1)	11.6843(1)	12.4091(5)	12.2982(3)
*M*1 in 48*f*	*x*	0.3194(4)	0.3159(1)	0.3139(4)	0.3143(5)
(*x* 1/8 1/8)	U_{iso}, Å^2	0.013(2)	0.0112(4)	0.004(1)	0.009(2)
	n	1.0(–)	1.0(–)	0.336(5)Ti	0.331(7)Ti
				0.664(5)Zr	0.669(7)Zr
*M*2 in 16*d*	U_{iso}, Å^2	0.01(–)	0.016(1)	0.01(–)	0.009(3)
(1/2 1/2 1/2)	*n*	0.854(4)Ti	0.948(3)Ti	0.993(5)Ti	1.0(–)Ti
		0.146(4)Fe	0.052(3)Fe	0.007(5)Zr	
Fe in 32*e*	*x*	0.7060(1)	0.70647(4)	0.70004(9)	0.7010(1)
(*x x x*)	U_{iso}	0.0152(8)	0.0088(3)	0.0094(4)	0.0142(8)
	n	1.0(–)	1.0(–)	1.0(–)	1.0(–)
O in 16*c*	U_{iso}, Å^2	0.018(5)	0.011(1)	0.01(–)	0.0141(5)
(0 0 0)	*n*	**0.348(7)**	**0.558(3)**	**0.24(1)**	**0.54(3)**
	r_i, Å	0.77	0.74	0.78	0.76
D1 in 32e	*x*	–	–	–	0.033(1)
(*x x x*)	U_{iso}, Å^2				0.026(1)
	n				**0.149(9)**
	r_i, Å				0.45
D(T1) in 32*e*	*x*	–	–	0.0648(5)	0.062(4)
(*x x x*)	U_{iso}, Å^2			0.0192(8)	0.026(1)
	n			**0.266(8)**	**0.048(9)**
	r_i, Å			0.36	0.35
D(T2) in 32*e*	*x*	–	–	0.185(4)	–
(*x x x*)	U_{iso}, Å^2			0.0192(8)	
	n			0.035(6)	
	r_i, Å			0.37	
D2 in 192*i*	*x*	0.492(3)	0.499(1)	0.4800(5)	0.4806(7)
(*x y z*)	*y*	0.575(3)	0.558(2)	0.5721(6)	0.5675(7)
	z	0.362(3)	0.352(1)	0.3617(5)	0.3621(6)
	U_{iso}, Å^2	0.019(1)	0.0146(7)	0.0192(8)	0.026(1)
	n	**0.038(3)**	**0.033(1)**	**0.217(2)**	**0.201(5)**
	r_i, Å	0.35	0.36	0.44	0.42
D3 in 96*g*	*x*	0.2788(2)	0.2792(1)	0.2839(2)	0.2810(4)
(*x x z*)	*z*	0.1496(2)	0.1515(2)	0.1566(4)	0.1554(5)
	U_{iso}, Å^2	0.019(1)	0.0146(7)	0.0192(8)	0.026(1)
	n	**0.652(7)**	**0.442(3)**	**0.566(5)**	**0.434(7)**
	r_i, Å	0.41	0.41	0.48	0.46
D7 in 8*a*	U_{iso}, Å^2	0.048(4)	0.036(1)	0.0192(8)	0.057(6)
(1/8 1/8 1/8)	*n*	**0.99(2)**	**0.990(8)**	**0.35(2)**	**0.81(4)**
	r_i, Å	0.83	0.77	0.80	0.77
R-factors	R_p, %	3.54	2.69	3.06	3.24
	R_{wp}, %	4.77	3.83	3.84	2.49
	χ^2	2.33	2.00	1.841	1.869
Refined composition		$Ti_{3.85(1)}Fe_{2.15(1)}$ $\times O_{0.35(1)}D_{4.87(9)}$	$Ti_{3.948(3)}Fe_{2.052(3)}\times$ $O_{0.558(3)}D_{3.54(3)}$	$Ti_{2.00(2)}Zr_{2.00(2)}Fe_2$ $\times O_{0.24(1)}D_{6.78(9)}$	$Ti_{1.99(2)}Zr_{2.01(2)}Fe_2$ $\times O_{0.54(3)}D_{5.8(2)}$
Refined D content per formula unit		4.87(9)	3.54(3)	6.78(9)	5.8(2)

Table 3 Distribution of hydrogen atoms among different interstices in η-$Ti_{4-x}Zr_xFe_2O_y$-based hydrides (deuterides).

Type of interstice	Surrounding of interstice	Number of hydrogen atoms per unit cell				
		$Ti_4Fe_2OD_{2.5}$	$Ti_4Fe_2O_{0.5}D_{3.5}$	$Ti_4Fe_2O_{0.25}D_{4.9}$	$Ti_2Zr_2Fe_2O_{0.5}D_{5.8}$	$Ti_2Zr_2Fe_2O_{0.25}D_{6.8}$
D1 (32e_1)	$(Ti,Zr)_3Fe$		–	–	4.77	–
T1 (32e_2)	$(Ti,Zr)_3$		–	–	–	1.12
T2 (32e_3)	$(Ti,Zr)_3$		–	–	1.54	8.51
D2 (192i)	$(Ti,Zr)_3Fe$	18.7	6.53	7.30	38.59	41.66
D3 (96g_1)	$(Ti,Zr)_3Fe$	8.7	41.95	62.59	41.66	54.34
D4 (96g_2)	$(Ti,Zr)_2Fe_2$		–	–	–	–
D5 (8b)	Fe_4		–	–	–	–
D6 (32e_4)	$(Ti,Zr)Fe_3$		–	–	–	–
D7 (8a)	$(Ti,Zr)_6$	8	8	8	6.48	2.83
D8 (16c)	$(Ti,Zr)_6$	–	–	–	–	–
Total amount of hydrogen atoms		35.4	56.48	77.86	93.04	108.46

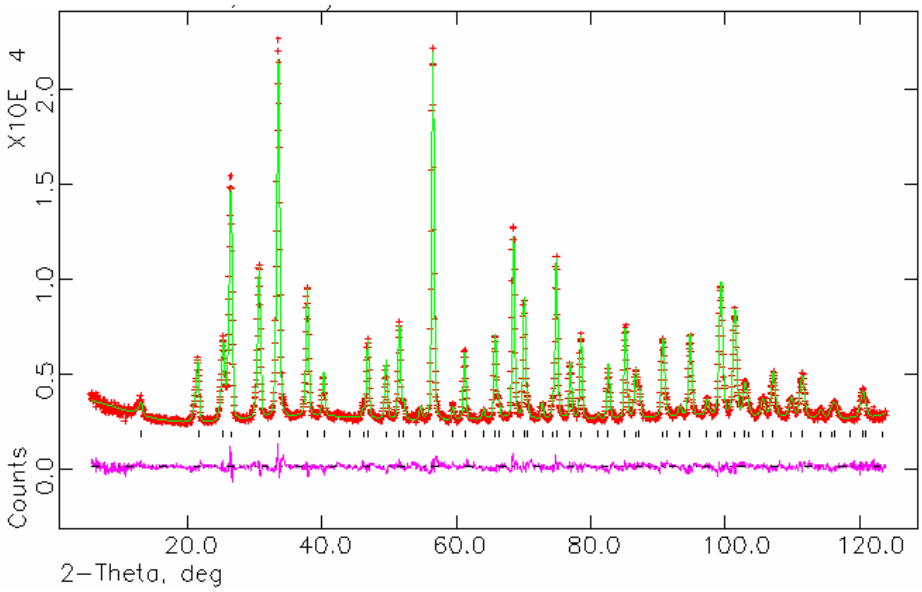

Fig. 4 Observed (+), calculated (line) and difference (bottom line) Rietveld profiles for powder neutron diffraction of the $Ti_4Fe_2O_{0.25}D_{4.9}$ deuteride (λ = 1,551 Å).

explained by blocking of the filling of D3 sites, which at 1 O at./f.u. become impossible. The decrease of the hydrogenation capacity observed with increasing oxygen content is accompanied by a substantial increase of the hydrogen-induced expansion of the unit cell. For the $Ti_4Fe_2O_{0.25}D_{4.9}$ deuteride it represents 1.77 Å^3, whereas for the $Ti_4Fe_2O_{0.5}H_{3.5}$ hydride it is equal to 2.51 Å^3, the volume of the initial unit cell of both compounds being almost equal. A similar effect was observed earlier for hydrogenation of Zr_3NiO_x alloys [22,23].

The presence of oxygen, in addition to inducing changes in the structure and hydrogenation properties, modifies some other physicochemical properties of the alloys as well: it facilitates activation of Ti–Fe alloys [5], and decreases the affinity of the Zr_2Fe compound

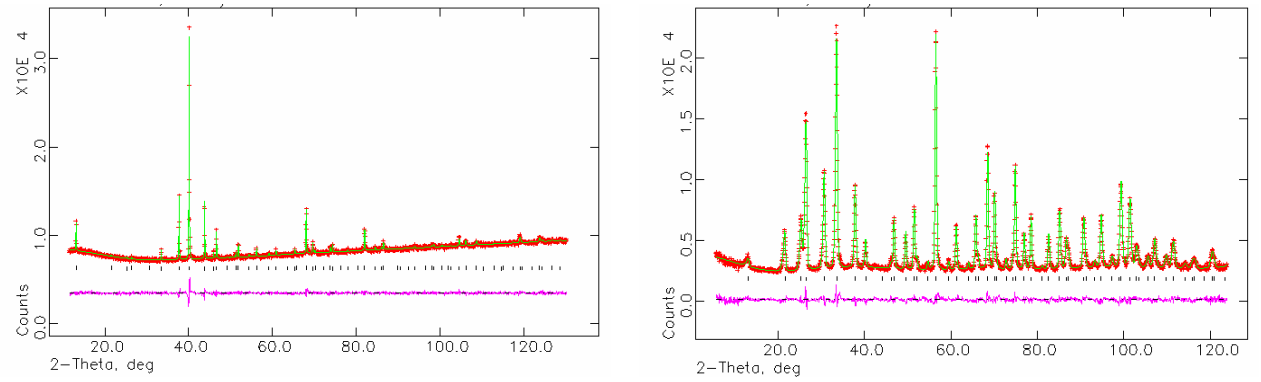

a *b*

Fig. 5 Observed (+), calculated (line) and difference (bottom line) Rietveld profiles of the $Ti_4Fe_2O_{0.5}D_{3.5}$ deuteride: XRD Cu Kα (a) and PND (λ = 1.551 Å) (b). Positions of Bragg's peaks are marked by vertical bars.

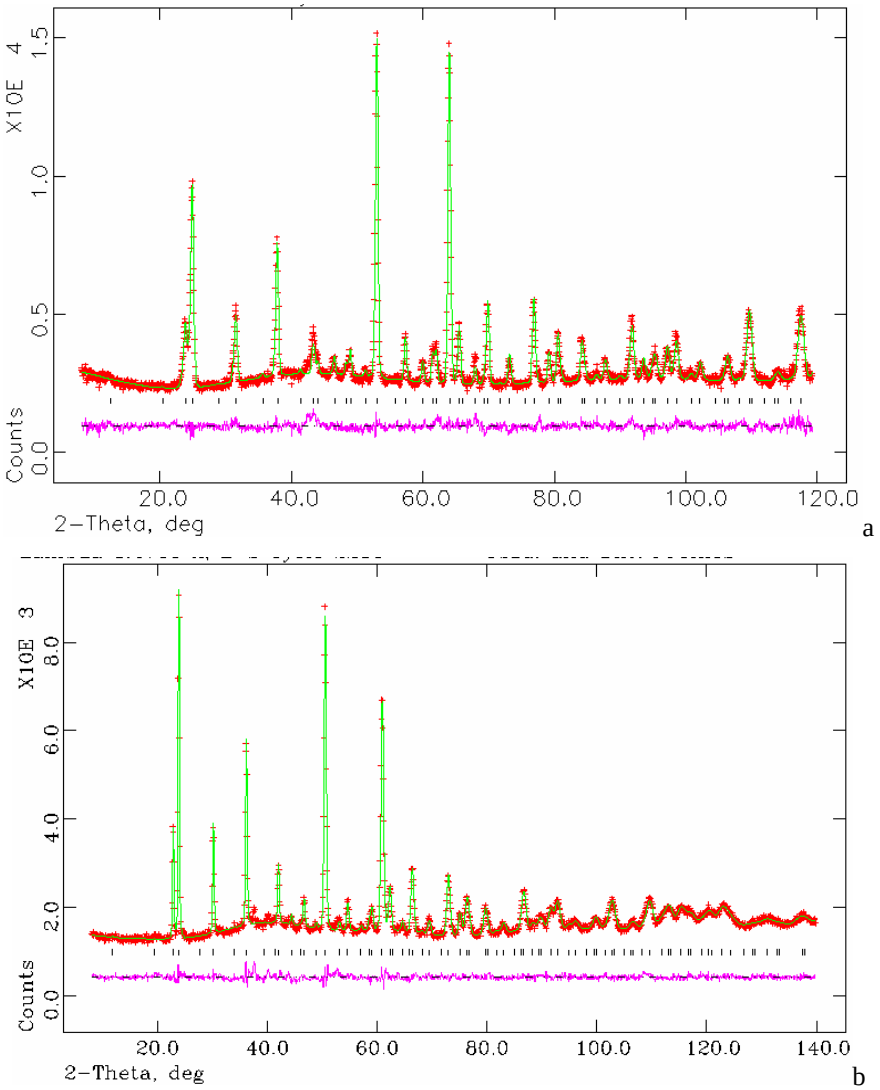

Fig 6 Observed (+), calculated (line) and differential (bottom line) Rietveld profiles for PND of $Ti_2Zr_2Fe_2O_{0.25}D_{7.2}$ (λ = 1.551 Å) (a) and $Ti_2Zr_2Fe_2O_{0.5}D_{5.8}$ (λ = 1.47 Å) (b) deuterides.

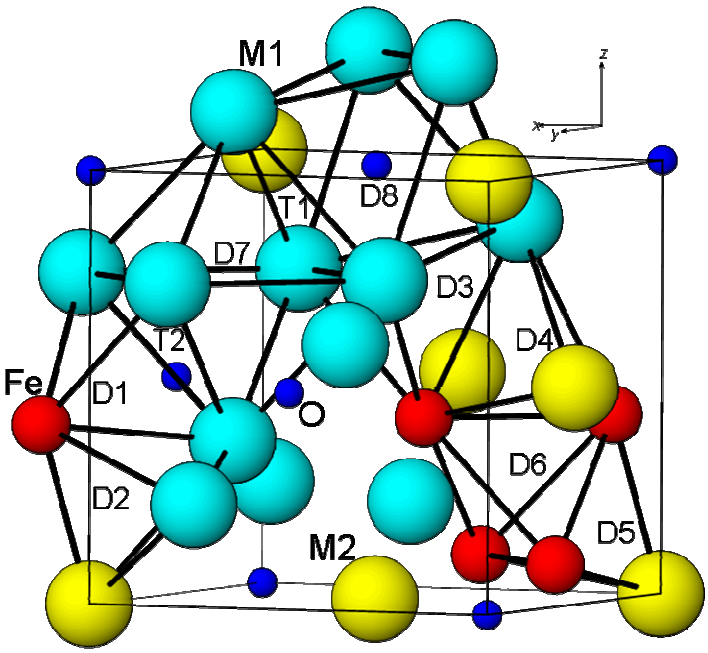

Fig. 7 Types of interstice in the structure of $(Ti,Zr)_4Fe_2O_x$.

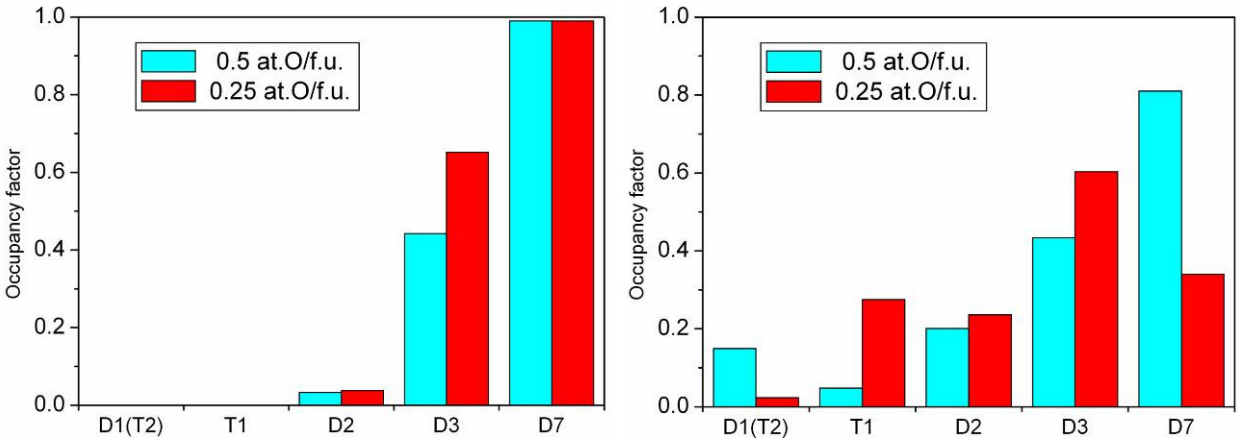

Fig. 8 Diagram of D-atom distribution in the structures of the deuterides $Ti_4Fe_2O_{0.25}D_{4.9}$ and $Ti_4Fe_2O_{0.5}D_{3.5}$ (a), $Ti_2Zr_2Fe_2O_{0.25}D_{7.2}$ and $Ti_2Zr_2Fe_2O_{0.5}D_{5.8}$ (b).

to disproportionation during hydrogen absorption-desorption cycling [12]. It order to verify the influence of the oxygen content on disproportionation we performed hydrogenation of $Ti_4Fe_2O_{0.25}$ and $Ti_4Fe_2O_{0.5}$ alloys at high temperatures. The first experiment, where the alloys were kept at 550°C under 0.1 MPa hydrogen gas for 5 hours did not cause any degradation – both $Ti_4Fe_2O_{0.25}$ and $Ti_4Fe_2O_{0.5}$ remained single-phase. However, under more severe hydrogenation conditions (0.5 MPa H_2 at 750°C for 2 hours) the sample with lower oxygen content partly disproportionated. XRD patterns of the freshly disproportionated material show that in addition to the main $Ti_4Fe_2O_x$ phase, three additional phases have appeared – TiH_2, TiO and TiFe (Fig. 9a). The sample with higher oxygen content under the same condition remained single-phase (Fig. 9b).

Conclusions

The existence of a continuous solid solution of η-phases between $Ti_4Fe_2O_x$ and $Zr_4Fe_2O_x$, confirmed in this work, makes it possible to modify the hydrogen absorption characteristics of these materials from getter ones (η-$Zr_4Fe_2O_x$) to those of typical hydrogen storage materials (η-$Ti_4Fe_2O_x$).

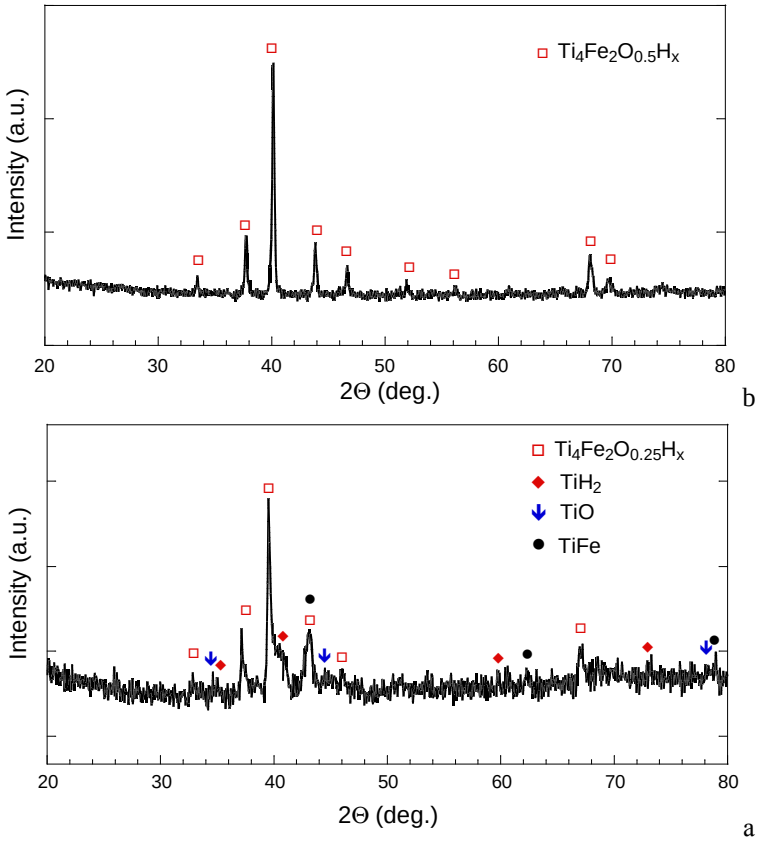

Fig. 9 X-ray diffraction profiles of $Ti_4Fe_2O_{0.25}$ (a) and $Ti_4Fe_2O_{0.5}$ (b) alloys after heat treatment in hydrogen at 750°C ($P(H_2)$ = 0.5 MPa, 2 hours).

The hydrogenation properties of a series of $Ti_{4-x}Zr_xFe_2O_y$ (x = 0, 1, 2, 3; y = 0.25, 0.5) η-suboxides have been studied. An increase of the Zr content in $(Ti,Zr)_4Fe_2O_{0.5}$ is accompanied by a monotonous increase of the unit cell dimensions, hydrogenation capacity and relative unit cell expansion, the symmetry of the parent compounds being retained during the hydrogenation.

The crystal structure of four deuterides: $Ti_4Fe_2O_{0.25}D_{4.9}$, $Ti_4Fe_2O_{0.5}D_{3.5}$, $Ti_2Zr_2Fe_2O_{0.25}D_{7.2}$, and $Ti_2Zr_2Fe_2O_{0.5}D_{5.8}$ has been investigated by both X-ray and neutron powder diffraction. In all these deuterides two types of $[(Ti,Zr)_3Fe]$ tetrahedron and one $[(Ti,Zr)_6]$ octahedron accommodate D atoms. In addition, in Zr-substituted deuterides the occupation of $[(Ti,Zr)_3]$ triangular faces was observed. All the studied structures are characterised by a disordered hydrogen sublattice.

Reduction in the O content at constant Ti/Zr ratio leads to increase in hydrogenation capacity, which can be attributed to **diminishing of the** O-H blocking effect (the most attractive sites for H atoms are located around the octahedron filled by O, thus with decreasing oxygen occupancy of this octahedron the number of sites available for H accommodation increases). High-temperature hydrogenation of $Ti_4Fe_2O_{0.25}$ and $Ti_4Fe_2O_{0.5}$ alloys revealed lower resistance against disproportionation for materials with lower oxygen content.

Acknowledgements

Travel funds from the Visby Programme of the Swedish Institute are gratefully acknowledged. We thank H. Rundlöf and A. Wannberg (Neutron Research Laboratory, Studsvik, Sweden) for skilled assistance with the PND data collection. Dr. I. Marchuk (Institute of Physical Chemistry, PAN, Warsaw, Poland) is thanked for assistance with XRD measurements.

References

[1] E.K. Molchanova, *Atlas of Phase Diagrams of Titanium Alloys*, Mashinostroyenie, Moscow, 1964, 390 p. (in Russian).

[2] T. Nambu, H. Ezaki, H. Yukawa, M. Morinaga, *J. Alloys Compd.* 293-295 (1999) 213-216.

[3] P. Fischer, J. Schefer, K. Yvon, L. Schlapbach, T. Riesterer, *J. Less-Common Met.* 129 (1987) 39-45.

[4] M. Mintz, Z. Hadari, M. Dariel, *J. Less-Common Met.* 74 (1980) 287-294.

[5] B. Rupp, *J. Less-Common Met.* 104 (1984) 51-63.
[6] B. Rupp, P. Fischer, *J. Less-Common Met.* 144 (1988) 275-281.
[7] C. Stioui, D. Fruchart, A. Rouault, R. Fruchart, E. Roudaut, J. Rebiére, *Mater. Res. Bull.* 16 (1981) 869-876.
[8] D. Arias, J.P. Abriata, *The Fe–Zr System*, In: T.B. Massalski (Eds.), *Binary Alloy Phase Diagrams*, 2nd Edition, ASM International, Materials Park, Ohio, 1990, Vol. 2, pp. 1798-1800.
[9] M.V. Nevitt, J.W. Downey, R.A. Morris, *Trans. Metall. Soc. AIME* 218 (1960) 1019-1023.
[10] P. Raj, P. Suryanarayana, A. Sathyamoorthy, K. Shashikala, R.M. Iyer, *J. Alloys Compd.* 178 (1992) 393-401.
[11] I.Yu. Zavaliy, A.O. Pecharsky, R. Cerny, P.Yu. Zavalij, W.B. Yelon, G. Wiesinger, V.K. Pecharsky, *Proc. 20th Eur. Crystallogr. Meet. (ECM'2001)*, Cracow, Poland, 2001, p. 304 (S8.M1.P17).
[12] I.Yu. Zavaliy, O. Gutfleisch, V.A. Yartys, I.R. Harris, *Proc. VII Int. Conf. Hydrogen Materials Science and Chemistry of Metal Hydrides*, Alushta, Kiev, Ukraine, 2001, pp. 336-339.
[13] I.Yu. Zavaliy, *J. Alloys Compd.* 291 (1999) 102-109.
[14] I.Yu. Zavaliy, A.B. Riabov, V.A. Yartys, G. Wiesinger, H. Michor, G. Hilscher, *J. Alloys Compd.* 265 (1998) 6-14.
[15] I.Yu. Zavaliy, G. Wóicik, G. Młynarek, I.V. Saldan, V.A. Yartys, M. Kopczyk, *J. Alloys Compd.* 314 (2001) 124-131.
[16] L.G. Akselrud, Yu.N. Grin, P.Yu. Zavalii, V.K. Pecharsky, V.S. Fundamensky, *Coll. Abstr. 12th Eur. Crystallogr. Meet.*, Moscow, 1989, Vol. 3, p. 155.
[17] A.C. Larson, R.B. von Dreele, *General Structure Analysis System*, LANL, Los Alamos, 1994.
[18] D.G. Westlake, *J. Less-Common Met.* 105 (1985) 69-81.
[19] F.J. Rotella, H.E. Flotow, D.M. Gruen, J.D. Jorgensen, *J. Chem. Phys.* 79(9) (1983) 4522-4531.
[20] D.G. Westlake, *J. Chem. Phys.* 79(9) (1983) 4532-4538.
[21] I.Yu. Zavaliy, W.B. Yelon, P.Y. Zavalij, I.V. Saldan, V.K. Pecharsky, *J. Alloys Compd.* 309 (2000) 75-82.
[22] I.Yu. Zavaliy, R. Cerny, I.V. Koval'chuck, I.V. Saldan, *J. Alloys Compd.* 360 (2003) 173-182.
[23] I.Yu. Zavaliy, R.V. Denys, R. Cerny, I.V. Koval'chuck, G. Wiesinger, G. Hilscher, *J. Alloys Compd.* 386 (2005) 26-34.